

# Time-Resolved Optical & Thermal Analyses of High-Power Laser Diode Arrays

Graham R. Allan, Aleksey Vasilyev, Elisavet Troupaki, Nasir Kashem and Mark A. Stephen.

NASA-Goddard Space Flight Center,  
Greenbelt, Maryland 20771. USA.

**Abstract** - Time-resolved optical and thermal analyses of laser diode arrays reveals temperature induced chirp and the presence of anomalous hot spots.

## I. INTRODUCTION

An important need, especially for space-borne applications, is the early identification and rejection of laser diode arrays which may fail prematurely. Temperature has been identified as an important parameter in the performance of a Laser Diode Arrays (LDA). The lifetime of LDAs decrease exponentially with increasing temperature[1]. This has led to the development of two techniques, temporally-resolved thermography, from which the time resolved temperature of the output facet of the device is measured and Temporally-resolved and Spectrally-Resolved (TSR) optical output from which the temperature of the active region of the device can be measured [2, 3]. This is in addition to power monitoring on long-term burn stations. A numerical model of the thermal properties of the device has also been constructed from which the time-evolution of heat flow through the device can be modeled for various conditions.

In this paper we briefly discuss the measurement setup and present temperature data derived from thermal images, numerical modeling and TSR data for two differently designed high-power 808 nm LDA packages of similar specification operated in an electrical and thermal environment that mimic the expected operational conditions.

## II. EXPERIMENTAL DESCRIPTION

The experimental setup for LDA characterization is shown in Figure 1. The LDA is mounted on a thermally controlled heat sink maintained at 25°C. The diode driver provides current pulses of up to 150A peak, between 50 $\mu$ s and 5ms duration, and a compliance voltage of up to 100V. The LDA drive current is monitored via a low-voltage current monitor built into the diode controller and DAQ card. Voltage across the diode is measured with a digital multimeter. The light from the laser diode array is collected by an integrating sphere. The optical power is monitored with a UDT S390 power meter calibrated with this integrating sphere. In addition there is a fiber optic port which couples light to an Agilent 86141B optical spectrum analyzer (OSA). Time-resolved emission measurements are made with the OSA set to "filter-mode", a fiber-coupled photodiode and digital oscilloscope. In filter-mode the OSA acts as a tunable, narrow, band-pass filter.

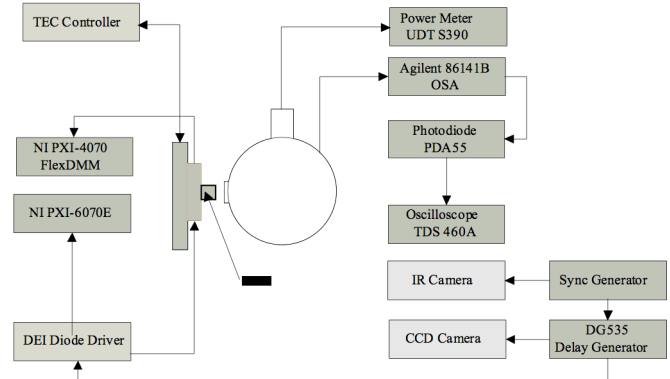


Fig. 1. Schematic of the measurement set up showing TSR instrumentation, MID-IR Camera and Near Field Camera.

To temporally and spatially resolve the temperature of the front facet of the LDA, a series of thermographic images was recorded. Thermal images are captured in the 3 to 5  $\mu$ m spectral region using a commercial mid-infrared camera. The camera has 320 x 256 InSb FPA (30 x 30  $\mu$ m pixel size) with a frame rate of 60Hz and an integration time of up to 1.7msec. The MID-IR camera has germanium 1x microscope lens, which gives a spatial resolution, limited by FPA pixel size, of 30 $\mu$ m. Temperature resolution is better than 25mK. To correctly capture the IR pulses it is important to synchronize the MID-IR camera to the diode pulses. Both the diode driver and MID-IR CCD camera are synchronized to the same reference signal through a digital delay generator. To obtain the temperature change one must subtract the cold background from the "hot" image. To do this accurately requires that the IR camera be used in an external synchronization mode.

The camera was triggered on both the rising and falling edges of each pulse providing 59.94 frames per second operation. The sync' signal was a 29.97Hz square wave with 50% duty cycle. The diode driver was synchronized with the same signal but was triggered only on the rising edge operating at 29.97Hz. We acquired a stream of 32 frames from the IR camera. Half of the frames in the stream captured the LDA while the current was applied to the diode, "On-cycle" thermograph images, and the other half captured LDA thermograph images after it was cooled, "Off-cycle" images. Numerically the averaged Off-cycle images were then subtracted from the averaged On-cycle images. By reducing the IR camera integration time from 1.7msec to 70 $\mu$ sec one can capture thermographic images on a finer time

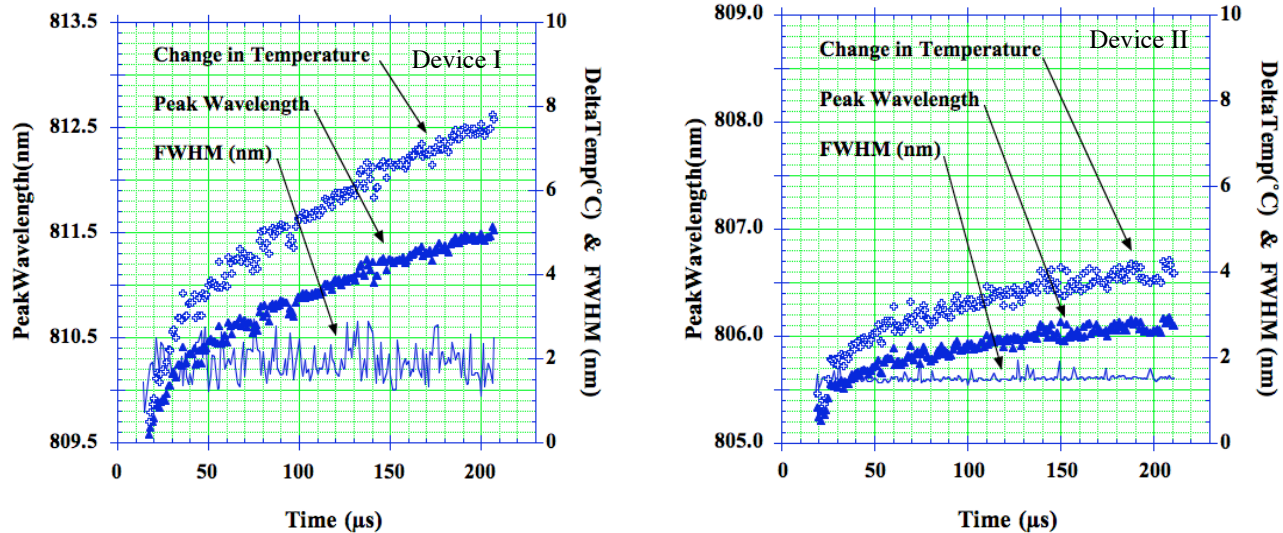


Fig. 2. Change in temperature, peak wavelength and FWHM as a function of time

scale and by varying the delay one can temporally resolve the front facet temperature through the current pulse and in to the off cycle. In this case the delay was changed in increments of by  $50\mu\text{sec}$ .

Near field images were also captured using a commercial, monochrome CCD camera sensitive to the 808 nm light. To avoid saturating the CCD it was necessary to attenuate the optical signal with ND filters.

The numerical models uses a finite element array which consists of three layers, the semiconductor layer sandwiched between two heat sinks. The model calculates the thermal gradients and energy flow within each layer and between the active region and the heatsink in each time step. This results in a time-resolved temperature map of the device. Anomalous hot regions can be created within the device and the effect on the system modeled.

### III. RESULTS AND DISCUSSION

Two high-power 808 nm, laser diode arrays with different mechanical package designs are measured and compared. Both devices are 4-bar arrays and each bar has  $\sim 70$  emitters.

The device under test was mounted on a temperature controlled heat sink, maintained at  $25^\circ\text{C}$  and allowed to come to thermal equilibrium while operating at 70A peak current, in  $200\mu\text{s}$  pulses at 30 Hz rep-rate producing approximately the same optical output power. The OSA was set to filter mode and the center of the filter stepped through the emission spectrum of the LDA. At each wavelength-setting the temporal profile of the intensity is recorded via the digitizing oscilloscope. The resulting data matrix was then analyzed to determine the peak wavelength as a function of time. The peak wavelength of these LDAs tunes  $\sim 0.27\text{nm}/^\circ\text{C}$ . The peak wavelength, Full Width Half Maximum (FWHM) and temperature, derived from the temporally resolved data matrix, are plotted in Figure 2. This representation of the

temporally resolved spectra clearly shows a temperature induced chirp to longer wavelengths. This chirp is attributed to the current pulse thermally tuning the device. The current pulse induces a bulk temperature rise of  $\sim +8^\circ\text{C}$  and a shift to longer wavelength of  $\sim 2\text{nm}$  by the end of the  $200\mu\text{s}$  pulse in the Device I. An approximately  $+4^\circ\text{C}$  change and just over  $+1\text{ nm}$  shift are induced in Device II. After the first  $30\mu\text{s}$  the heating is linear with time consistent with a constant rate of heating.

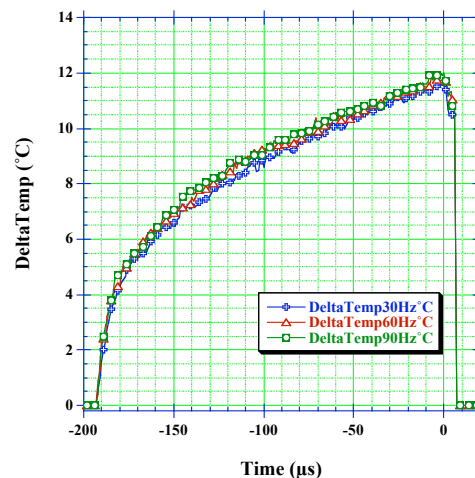


Fig. 3. Plotted are the measured temperature change derived from the shift in peak wavelength at three rep-rates; 30 Hz, 60 Hz and 90 Hz.

The spectral FWHM, to within the measurement ( $0.1\text{ nm}$ ), does not change during the pulse. Device II, under the same measurement conditions shows a much lower temperature rise, again with no discernable change in the spectral width. This LDA should, all other considerations being equal, have a longer mean-time between failures due the lower thermally induced stress[4]. Also studied was the temperature rise for different operational rep-rate but at the same heat sink temperature.

Figure 3 plots the induced temperature rise derived from the wavelength chirp for 30, 60 and 90 Hz rep-rate. The temperature of the device was maintained at 25°C and the peak current pulse increased to 100A. The temperature change due to the drive pulse is shown to be essentially independent of frequency for these low rep-rates. However the device may exhibit a slight bias to higher temperatures at higher rep-rates. The overall, larger, change in temperature, compared to figure 2 is due to the higher peak current.

It is important to note that all these data represent the spatially averaged output of all the laser diode emitters and thus the average temperature of all the active regions. As can be seen from the near field image of the LDA, figure 4, there is variability in the emitter strength. This image was taken by the Si-CCD camera and gives the relative strength of the individual emitter.



Fig. 4. Nearfield image of the laser diode array under normal operation. Each bright dash is one emitter. This device has four rows of emitters.

Figure 5, clearly shows a spatially resolved temperature rise of the LDA at one instant during the pulse. One can clearly see the four bar construction of the devices. It also reveals the locations of several hot spots not observed by TSR or nearfield image. The actual temperature rise can be calculated after corrections for emissivity and relative duty cycle are applied. From the time-resolved image sequence taken with this LDA the temperature of the three hot spots were recorded as a function of time and plotted in figure 6. Current pulse-on is  $\sim 300 \mu s$ , current pulse -off is  $\sim 500 \mu s$ . Clearly the growth of two hot spot continues after the current pulse has turned off, indicating the hot spot lies deeper within the device. After the temperature peaks the temperature decline has a simple exponential decay. Interestingly the time constant for Hot spot #3 is much longer than spots 1 or 2.

#### IV. NUMERICAL MODELING

The numerical model was used to predict the behavior of the front face temperature as a function of hot-spot position within the semiconductor layer. Four numerical runs are plotted in figure 7 for a hot-spot generated just inside the front face, one quarter of the way into the sample, the middle of the sample and the three quarters of the way through the sample. The hot spot was created for the duration of the current pulse and was maintained at the same elevated temperature. The maximum temperature of the front face was then recorded as a function of time. Only when the

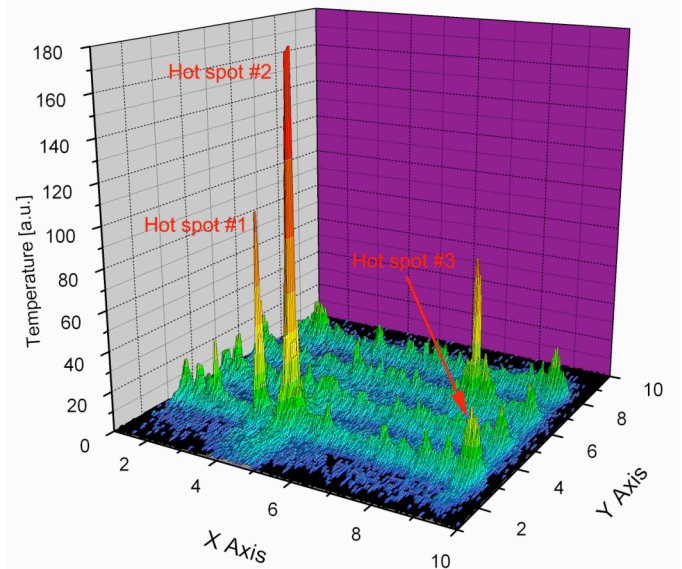


Fig. 5. Time resolved image of the front facet temperature approximately 180  $\mu s$  after turn-on of the current pulse. Three anomalous temperature regions are identified, Hot spots 1, 2 & 3.

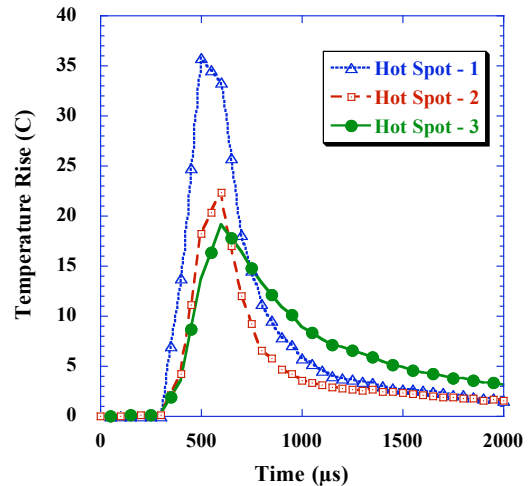


Fig. 6. The temporal evolution of the temperature of the three identified hot spots is plotted as a function of time. Current pulse-on is  $\sim 300 \mu s$ , current pulse-off is  $\sim 500 \mu s$ . Clearly the growth of two hot spot continues after the current pulse has turned off indicating the hot spot lies within the device.

hotspot was modeled near the front surface did the temperature decay when the current pulse was turned-off. When the temperature continues to rise after the current is turned off indicates that the hot spot is deeper within the sample. Figure 8 is a semilog plot of an overlay of the predicted temperature for a hotspot just inside the front face of the sample with the time resolved behavior of the feature. Interestingly the time constant for Hot spot #3 is much longer than the model predicts and will require further examination.

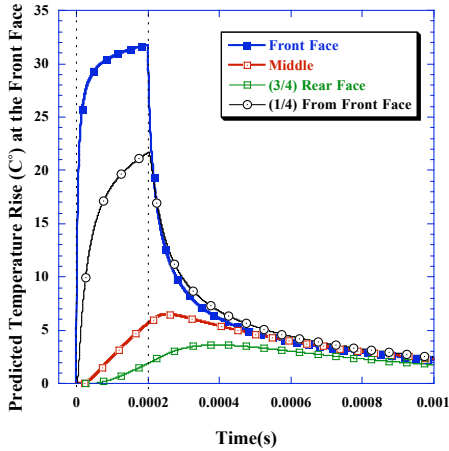


Fig. 7. The predicted front face temperature as a function of time for a hot-spot generated just inside the front face, one quarter of the way into the sample, the middle and the three quarters of the way through the sample.

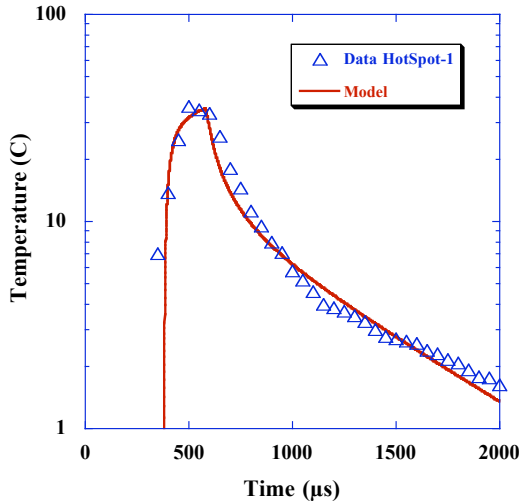


Fig. 8. Semilog plot of an overlay of the predicted temperature for a hotspot just inside the front face of the sample with the time resolved behavior of the feature.

## V. CONCLUSION

From the temporally and spectrally resolved output from the LDA one can directly measure the increase in temperature of the active region of the LDA. These data are used with the time-resolved thermographic images to measure the spatial distribution and magnitude of the temperature change. The time-resolved infrared images taken in the 3-5  $\mu\text{m}$  optical band can clearly show the presence of anomalous hot-spots within the normal thermal features of the array. Numerical modeling indicates the spots are near the front facet. These techniques may prove useful in helping to predict early failures of laser diode arrays.

## REFERENCES

- [1] Mitsuo Fukuda, *Reliability and degradation of semiconductor laser and LEDs*, Boston, MA: Artech House, c1991. ISBN 0890064652.
- [2] M. Voss, C. Lier, U. Menzel, A. Barwolff and T. Elsaesser, "Time-resolved emission studies of GaAs/AlGaAs laser diode arrays on different heat sinks", *J. Appl. Phys.* **79**(2), 15 January 1996. pp 1170-1172
- [3] Alex Vasilyev, Graham R. Allan, John Schafer, mark A. Stephen and Stefano Young, "Optical & Thermal Analyses of High-Power Laser Diode Arrays", *Technical Digest, Seventeenth Solid State and Diode Laser Technology Review*, p-38, 8-10 June, 2004 Albuquerque, New Mexico.
- [4] A. Gerhardt, F. Weik, Tien Quoc Tran, J. W. Tomm, T Elsaesser, J. Biesenbach, H. Muntz, G. Seibold and M. L. Biermann, "Device deformation during low-frequency pulsed operation of high-power diode bars". *Applied Physics Letters*, V84, Number 18, 3 May 2004, pp 3525-3527.